To identify putative biomarkers of the pharmacodynamic effects of ZD6474 *in vivo*, we identified 28 candidate genes from implanted 58As1 tumor samples by oligonucleotide microarray analysis (Fig. 4*a*). IGFBP-3 has multiple functions, including in the induction of apoptosis,[23] the inhibition of cancer cell proliferation,[24] and carcinogenesis[25] and IGFBP-3 expression is transcriptionally upregulated under hypoxic conditions.[26] A recent study has also shown that EGFR regulates IGFBP-3 expression and secretion.[27] The inhibitory effect of ZD6474 on EGFR kinase may be associated with the upregulation of IGFBP-3. ADM, which was first identified in a human pheochromocytoma, is known to regulate circulation by acting as a hormone.[28] Adrenomedullin is also induced by hypoxia and may have a role in protecting against hypoxic cellular damage in human retinal pigment epithelial cells.[29] Expressions of nine of the upregulated genes, *IGFBP-3*, *ADM*, *ANGPTL4*, *PLOD2*, *DSIPI*, *NDRG1*, *ENO2*, *HIG2* and *BNIP3L*, has been reported previously to be induced by hypoxia.[26,29–38] We hypothesize that ZD6474 inhibits neovascularization in tumors, thereby limiting the oxygen and nutrient supply and resulting in tumor hypoxia and upregulation of hypoxia-inducible genes. If this hypothesis is correct, hypoxia-regulated genes and gene products might be useful biomarkers for the pharmacodynamic effects of ZD6474 and other anti-angiogenic agents in preclinical and clinical settings. We are now investigating whether these genes and gene products can be used as biomarkers for the efficacy of ZD6474 in a correlative study.

Future directions of our study include: (*i*) to compare the antitumor effect of other "anti-vascular agents" with ZD6474 in this model; (*ii*) to evaluate combination therapy with ZD6474 plus anticancer agents; (*iii*) to evaluate the antitumor effect of ZD6474 against micro-metastasis *in vivo*; and (*iv*) to confirm the usefulness of the 9 candidate genes as biomarkers in clinically.

In conclusion, we demonstrated that ZD6474 inhibited tumor growth, suppressed intraperitoneal dissemination, and prolonged survival in a highly metastatic orthotopic gastric cancer model. We carried out a microarray analysis of tumor samples and we identified 9 hypoxia-inducible genes as candidate biomarkers for monitoring the effects of ZD6474 therapy. These findings provide a strong preclinical rationale for investigating ZD6474 for the treatment of gastric cancer in the clinic.

Acknowledgements

Grants were received from the 3rd-Term Comprehensive 10-Year Strategy for Cancer Control and from a Grant-in-Aid for Scientific Research from the Ministry of Education, Culture, Sports, Science and Technology of Japan (Grant number: 12217165). T.A. is the Recipient of a Research Resident Fellowship from the Foundation of Promotion of Cancer Research in Japan.

References

1. Vanhoefer U, Rougier P, Wilke H, Ducreux MP, Lacave AJ, Van Cutsem E, Planker M, Santos JG, Piedbois P, Paillot B, Bodenstein H, Schmoll HJ, et al. Final results of a randomized phase III trial of sequential high-dose methotrexate, fluorouracil, and doxorubicin versus etoposide, leucovorin, and fluorouracil versus infusional fluorouracil and cisplatin in advanced gastric cancer: A trial of the European Organization for Research and Treatment of Cancer Gastrointestinal Tract Cancer Cooperative Group. J Clin Oncol 2000;18:2648–57.
2. Ohtsu A, Shimada Y, Shirao K, Boku N, Hyodo I, Saito H, Yamamichi N, Miyata Y, Ikeda N, Yamamoto S, Fukuda H, Yoshida S. Randomized phase III trial of fluorouracil alone versus fluorouracil plus cisplatin versus uracil and tegafur plus mitomycin in patients with unresectable, advanced gastric cancer: the Japan Clinical Oncology Group Study (JCOG9205). J Clin Oncol 2003;21:54–9.
3. Moriguchi S, Kamakura T, Odaka T, Nose Y, Maehara Y, Korenaga D, Sugimachi K. Clinical features of the differentiated and undifferentiated types of advanced gastric carcinoma: univariate and multivariate analyses. J Surg Oncol 1991;48:202–6.
4. Ferrara N, Davis-Smyth T. The biology of vascular endothelial growth factor. Endocr Rev 1997;18:4–25.
5. Nicosia RF. What is the role of vascular endothelial growth factor-related molecules in tumor angiogenesis? Am J Pathol 1998;153:11–6.
6. Mustonen T, Alitalo K. Endothelial receptor tyrosine kinases involved in angiogenesis. J Cell Biol 1995;129:895–8.
7. Shibuya M. Vascular endothelial growth factor receptor-2: its unique signaling and specific ligand, VEGF-E. Cancer Sci 2003;94:751–6.
8. Manley PW, Bold G, Bruggen J, Fendrich G, Furet P, Mestan J, Schnell C, Stolz B, Meyer T, Meyhack B, Stark W, Strauss A, et al. Advances in the structural biology, design and clinical development of VEGF-R kinase inhibitors for the treatment of angiogenesis. Biochim Biophys Acta 2004;1697:17–27.
9. Hurwitz H, Fehrenbacher L, Novotny W, Cartwright T, Hainsworth J, Heim W, Berlin J, Baron A, Griffing S, Holmgren E, Ferrara N, Fyfe G, et al. Bevacizumab plus irinotecan, fluorouracil, and leucovorin for metastatic colorectal cancer. N Engl J Med 2004;350:2335–42.
10. Wedge SR, Ogilvie DJ, Dukes M, Kendrew J, Chester R, Jackson JA, Boffey SJ, Valentine PJ, Curwen JO, Musgrove HL, Graham GA, Hughes GD, et al. ZD6474 inhibits vascular endothelial growth factor signaling, angiogenesis, and tumor growth following oral administration. Cancer Res 2002;62:4645–55.
11. Ciardiello F, Caputo R, Damiano V, Troiani T, Vitagliano D, Carlomagno F, Veneziani BM, Fontanini G, Bianco AR, Tortora G. Antitumor effects of ZD6474, a small molecule vascular endothelial growth factor receptor tyrosine kinase inhibitor, with additional activity against epidermal growth factor receptor tyrosine kinase. Clin Cancer Res 2003;9:1546–56.
12. Sandstrom M, Johansson M, Andersson U, Bergh A, Bergenheim AT, Henriksson R. The tyrosine kinase inhibitor ZD6474 inhibits tumour growth in an intracerebral rat glioma model. Br J Cancer 2004;91:1174–80.
13. McCarty MF, Wey J, Stoeltzing O, Liu W, Fan F, Bucana C, Mansfield PF, Ryan AJ, Ellis LM. ZD6474, a vascular endothelial growth factor receptor tyrosine kinase inhibitor with additional activity against epidermal growth factor receptor tyrosine kinase, inhibits orthotopic growth and angiogenesis of gastric cancer. Mol Cancer Ther 2004;3:1041–8.
14. Taguchi F, Koh Y, Koizumi F, Tamura T, Saijo N, Nishio K. Anticancer effects of ZD6474, a VEGF receptor tyrosine kinase inhibitor, in gefitinib (Iressa) sensitive and resistant xenograft models. Cancer Sci 2004;95:984–9.
15. Arao T, Fukumoto F, Takeda M, Tamura T, Saijo N, Nishio K. Small in-frame deletion in the epidermal growth factor receptor as a target for ZD6474. Cancer Res 2004;64:9101–4.
16. Yanagihara K, Tanaka H, Takigahira M, Ino Y, Yamaguchi Y, Toge T, Sugano K, Hirohashi S. Establishment of two cell lines from human gastric scirrhous carcinoma that possess the potential to metastasize spontaneously in nude mice. Cancer Sci 2004;95:575–82.
17. Yanagihara K, Takigahira M, Tanaka H, Komatsu T, Fukumoto H, Koizumi F, Nishio K, Ochiya T, Ino Y, Hirohashi S. Development and biological analysis of peritoneal metastasis mouse models for human scirrhous stomach cancer. Cancer Sci 2005;6:323–32.
18. Lynch TJ, Bell DW, Sordella R, Gurubhagavatula S, Okimoto RA, Brannigan BW, Harris PL, Haserlat SM, Supko JG, Haluska FG, Louis DN, Christiani DC, et al. Activating mutations in the epidermal growth factor receptor underlying responsiveness of non-small-cell lung cancer to gefitinib. N Engl J Med 2004;350:2129–39.
19. Paez JG, Janne PA, Lee JC, Tracy S, Greulich H, Gabriel S, Herman P, Kaye FJ, Lindeman N, Boggon TJ, Naoki K, Sasaki H, et al. EGFR mutations in lung cancer: correlation with clinical response to gefitinib therapy. Science 2004;304:1497–500.
20. Pao W, Miller V, Zakowski M, Doherty J, Politi K, Sarkaria I, Singh B, Heelan R, Rusch V, Fulton L, Mardis E, Kupfer D, et al. EGF receptor gene mutations are common in lung cancers from "never smokers" and are associated with sensitivity of tumors to gefitinib and erlotinib. Proc Natl Acad Sci USA 2004;101:13306–11.
21. Yang SH, Lin JK, Lai CR, Chen CC, Li AF, Liang WY, Jiang JK. Risk factors for peritoneal dissemination of colorectal cancer. J Surg Oncol 2004;87:167–73.
22. Folkman J. What is the evidence that tumors are angiogenesis dependent? J Natl Cancer Inst 1990;82:4–6.
23. Kim HS, Ingermann AR, Tsubaki J, Twigg SM, Walker GE, Oh Y. Insulin-like growth factor-binding protein 3 induces caspase-dependent apoptosis through a death receptor-mediated pathway in MCF-7 human breast cancer cells. Cancer Res 2004;64:2229–37.
24. Kirman I, Poltoratskaia N, Sylla P, Whelan RL. Insulin-like growth factor-binding protein 3 inhibits growth of experimental colocarcinoma. Surgery 2004;136:205–9.

25. Renehan AG, Zwahlen M, Minder C, O'Dwyer ST, Shalet SM, Egger M. Insulin-like growth factor (IGF)-I, IGF binding protein-3, and cancer risk: systematic review and meta-regression analysis. Lancet 2004;363:1346–53.
26. Koong AC, Denko NC, Hudson KM, Schindler C, Swiersz L, Koch C, Evans S, Ibrahim H, Le QT, Terris DJ, Giaccia AJ. Candidate genes for the hypoxic tumor phenotype. Cancer Res 2000;60: 883–7.
27. Takaoka M, Harada H, Andl CD, Oyama K, Naomoto Y, Dempsey KL, Klein-Szanto AJ, El-Deiry WS, Grimberg A, Nakagawa H. Epidermal growth factor receptor regulates aberrant expression of insulin-like growth factor-binding protein 3. Cancer Res 2004;64:7711–23.
28. Hirata Y, Hayakawa H, Suzuki Y, Suzuki E, Ikenouchi H, Kohmoto O, Kimura K, Kitamura K, Eto T, Kangawa K. Mechanisms of adrenomedullin-induced vasodilation in the rat kidney. Hypertension 1995;25:790–5.
29. Udono T, Takahashi K, Nakayama M, Yoshinoya A, Totsune K, Murakami O, Durlu YK, Tamai M, Shibahara S. Induction of adrenomedullin by hypoxia in cultured retinal pigment epithelial cells. Invest Ophthalmol Vis Sci 2001;42:1080–6.
30. Le Jan S, Amy C, Cazes A, Monnot C, Lamande N, Favier J, Philippe J, Sibony M, Gasc JM, Corvol P, Germain S. Angiopoietin-like 4 is a proangiogenic factor produced during ischemia and in conventional renal cell carcinoma. Am J Pathol 2003;162:1521–8.
31. Hofbauer KH, Gess B, Lohaus C, Meyer HE, Katschinski D, Kurtz A. Oxygen tension regulates the expression of a group of procollagen hydroxylases. Eur J Biochem 2003;270:4515–22.
32. Khvatova EM, Samartzev VN, Zagoskin PP, Prudchenko IA, Mikhaleva II. Delta sleep inducing peptide (DSIP): effect on respiration activity in rat brain mitochondria and stress protective potency under experimental hypoxia. Peptides 2003;24:307–11.
33. Cangul H. Hypoxia upregulates the expression of the NDRG1 gene leading to its overexpression in various human cancers. BMC Genet 2004;5:27.
34. Szturmowicz M, Burakowski J, Tomkowski W, Sakowicz A, Filipecki S. Neuron-specific enolase in non-neoplastic lung diseases, a marker of hypoxemia? Int J Biol Markers 1998;13:150–3.
35. Denko N, Schindler C, Koong A, Laderoute K, Green C, Giaccia A. Epigenetic regulation of gene expression in cervical cancer cells by the tumor microenvironment. Clin Cancer Res 2000;6:480–7.
36. Kenny PA, Enver T, Ashworth A. Receptor and secreted targets of Wnt-1/beta-catenin signalling in mouse mammary epithelial cells. BMC Cancer 2005;5:3.
37. Fei P, Wang W, Kim SH, Wang S, Burns TF, Sax JK, Buzzai M, Dicker DT, McKenna WG, Bernhard EJ, El-Deiry WS. Bnip3L is induced by p53 under hypoxia, and its knockdown promotes tumor growth. Cancer Cell 2004;6:597–609.
38. Sowter HM, Ratcliffe PJ, Watson P, Greenberg AH, Harris AL. HIF-1-dependent regulation of hypoxic induction of the cell death factors BNIP3 and NIX in human tumors. Cancer Res 2001;61: 6669–73.

Skeletal Radiol
DOI 10.1007/s00256-005-0037-5

CASE REPORT

Mototaka Miyake
Ukihide Tateishi
Tetsuo Maeda
Yasuaki Arai
Kunihiko Seki
Tadashi Hasegawa
Kazuro Sugimura

Sclerosing perineurioma: tumor of the hand with a short T2

Received: 2 June 2005
Revised: 17 August 2005
Accepted: 17 August 2005

M. Miyake · U. Tateishi (✉) ·
T. Maeda · Y. Arai
Division of Diagnostic Radiology
and Nuclear Medicine,
National Cancer Center Hospital,
5-1-1, Tsukiji, Chuo-ku,
104-0045 Tokyo, Japan
e-mail: utateish@ncc.go.jp
Tel.: +81-3-35422511
Fax: +81-3-35423815

K. Seki
Division of Pathology,
National Cancer Center Hospital,
Tokyo, Japan

T. Hasegawa
Department of Clinical Pathology,
Sapporo Medical University
School of Medicine,
Sapporo, Japan

K. Sugimura
Department of Radiology,
Kobe University Graduate
School of Medicine,
Kobe, Japan

Abstract We present two cases of sclerosing perineurioma, a rare soft tissue tumor, in the palm and the ring finger respectively, presenting as a small, painless and subcutaneous mass. This tumor has a predilection for the digits and palms of young, predominantly male adults. In the present cases the tumors showed very low signal intensity on T2-weighted magnetic resonance (MR) images. Histologically they contained abundant collagen and hyalinized stroma, which would account for areas of low signal intensity on T2-weighted MR images. Immunohistochemically, the tumor cells were positive for vimentin, epithelial membrane antigen and human erythrocyte glucose transporter 1 and negative for S-100 protein. To the best of our knowledge, the appearance of sclerosing perineurioma on MR imaging has not been previously reported in the English-language literature. Sclerosing perineurioma should be considered in the differential diagnosis of hand tumors when the tumor shows low signal intensity on T2-weighted MR images.

Keywords Sclerosing perineurioma · Hand · MRI · Short T2

Introduction

Perineurioma is a rare soft tissue tumor composed of cells resembling those of the normal perineurium. It was first described in 1978 by Lazarus and Trombetta on the basis of ultrastructural findings [1]. There are two distinct forms of perineurioma, the intraneural and the extraneural; the latter is known as soft tissue perineurioma. Sclerosing perineurioma, first described by Fetsch and Miettinen in 1997, is an unusual variant of soft tissue perineurioma that presents as a small, painless, dermal or subcutaneous mass with a strong predilection for the digits and palms of young adults, predominantly males [2]. To the best of our knowledge, the appearance on magnetic resonance imaging (MRI) of sclerosing perineurioma has not been previously reported in the English-language literature. We report the MRI features of two cases of sclerosing perineurioma and correlate the MR findings with histological features.

Case report

Case 1

An 11-year-old girl presented with a 1- year history of a slowly growing painless mass in her left palm. Physical examination revealed a well-delineated elastic and hard mass

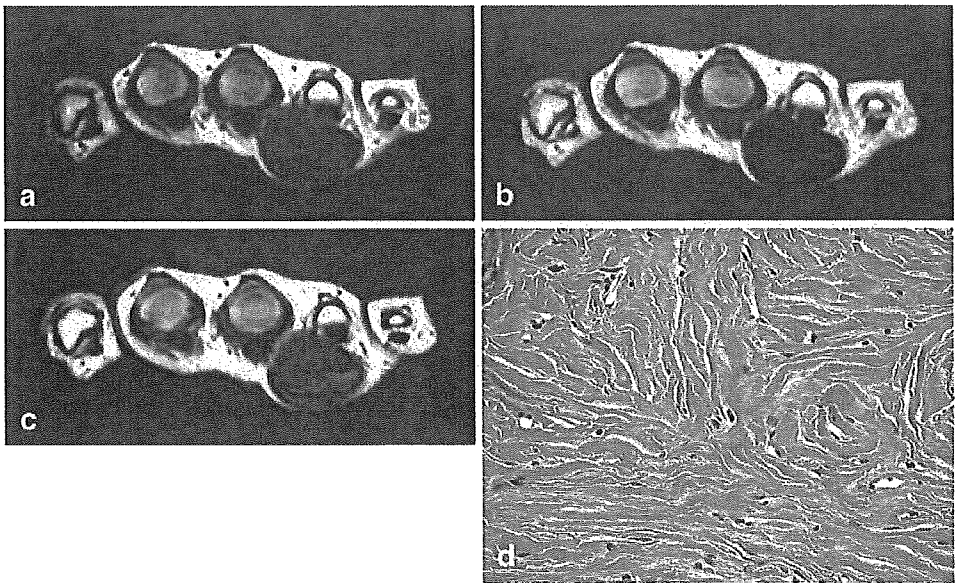

Fig. 1 An 11-year-old girl with a painless mass in her left palm. **a** Axial T1-weighted SE MR image (TR/TE 440/25) shows an iso signal intensity mass to that of muscle, in her left palm. **b** Axial T2-weighted FSE MR image (TR/TE 4000/87.3) reveals homogenously very low signal intensity of the mass. **c** Axial gadolinium-enhanced T1-weighted SE MR image suppression shows partial enhancement. **d** Photomicrograph of the tumor shows small, oval epithelioid or plump spindle cells, scattered and arranged in a corded and whorled pattern in abundant collagenous background. (H&E, ×40)

in her left palm and no limitation of finger motion. Radiographs showed a soft tissue mass in her left palm without erosion of adjacent bone. MRI of the left hand revealed a well-delineated mass measuring maximally 25×28 mm between the flexor tendons of the middle and ring fingers. The mass appeared homogeneous with signal intensity similar to that of muscle on T1-weighted spin echo (SE) MR images (Fig. 1a). On T2-weighted fast spin echo (FSE) MR images, the mass showed homogeneous low signal intensity similar to that of the tendons (Fig. 1b). On gadolinium-enhanced T1-weighted SE MR images with fat suppression, the mass showed partial slight enhancement (Fig. 1c). The margin of the mass displayed low signal intensity on all MRI pulse sequences, suggestive of a capsule or pseudocapsule. An excisional biopsy was performed. Grossly, the tumor was firm, well circumscribed and surrounded by a thin fibrous pseudocapsule. The cut surface of the tumor was solid, whitish and homogeneous in appearance.

Histologic examination revealed abundant collagenous tissue and small, oval epithelioid or plump spindle cells scattered and arranged in a corded, whorled or trabecular pattern (Fig. 1d). Small foci of necrosis, that is, ischemic infarction—possibly as a result of thrombosis—were identified (not shown). Cellular and nuclear atypia was rare and mitoses were not present. Tumor cells were positive for vimentin and epithelial membrane antigen (EMA) and negative for S-100 protein. In addition, they were diffusely and strongly positive for human erythrocyte glucose transporter 1 (GLUT1) with intensity similar to that of erythrocytes in tissue sections. The histological diagnosis of sclerosing perineurioma was made. After simple excision, there has been no evidence of recurrence or metastasis for 4 years, 4 months.

Case 2

A 16-year-old male presented with a painless and firm mass on the palmar side of his left ring finger. The mass slightly limited the range of motion of his ring finger. Laboratory tests showed no abnormalities. MRI of the left hand revealed a clearly defined mass measuring maximally 40×25 mm along the flexor tendon of his left ring finger. The lesion showed homogenously low to iso signal intensity relative to muscle on T1-weighted SE MR images (Fig. 2a) and very low signal intensity, similar to the tendons, on T2-weighted FSE MR images (Fig. 2b). On gadolinium-enhanced T1-weighted SE MR images, the lesion showed heterogeneous enhancement (Fig. 2c). On MRI, the tumor was attached to the flexor tendon of the left ring finger and there were no tendinous abnormalities. The patient underwent an excisional biopsy. Although the tumor was exophytically attached to the flexor digitorum profundus tendon of the left ring finger, there was no encasement of the flexor digitorum profundus tendon. The tumor was completely excised and the flexor tendon was preserved. Microscopic examination showed abundant collagen, which was partially sclerosed and hyalinized. In the collagenous background, there were small, oval epithelioid or plump spindle cells scattered and arranged

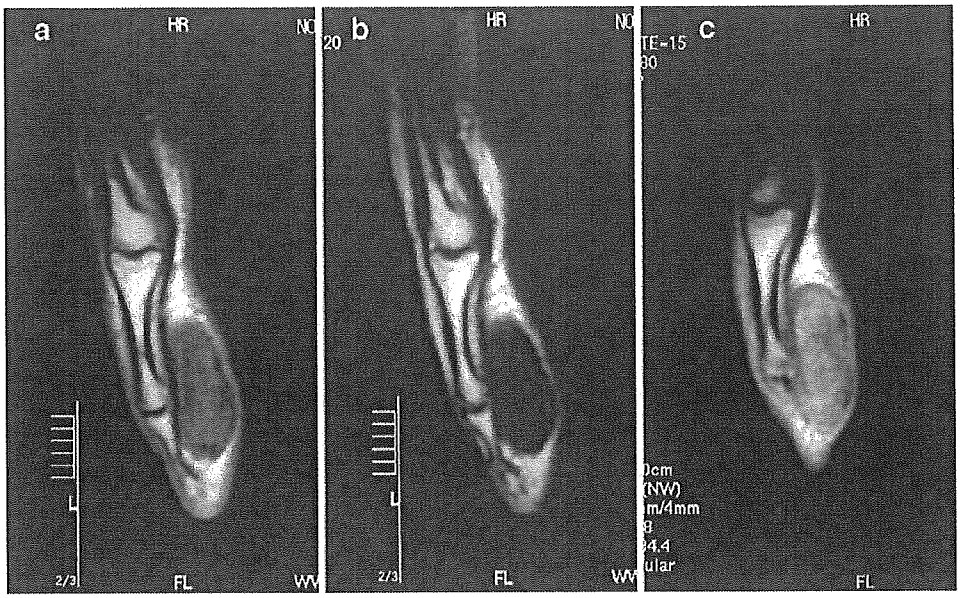

Fig. 2 A 16-year-old male with a painless mass in his left ring finger. **a** Sagittal T1-weighted SE MR image (TR/TE 440/25) shows a low- to iso-signal-intensity mass in comparison with muscle. **b** Sagittal T2-weighted FSE MR image (4500/120) reveals homogeneously very low signal intensity to the mass. **c** Sagittal gadolinium-enhanced T1-weighted SE MR image (500/15) with fat suppression shows heterogeneous enhancement

in a corded, whorled or trabecular pattern. Tumor cells were diffusely and strongly positive for GLUT1 and diffusely positive for vimentin and EMA. These histological findings were consistent with sclerosing perineurioma. On follow-up at 2 years, 2 months, there was no evidence of recurrence or metastasis.

Discussion

Sclerosing perineurioma is a rare soft tissue tumor composed of cells resembling those of the normal perineurium. It presents as a small, painless, dermal or subcutaneous mass with a strong predilection for the digits and palms of young adults [2]. Why this tumor has a marked predilection for the hands of young adults is unknown. The predominant chief complaint is a painless but slowly growing mass, which may range in size from 0.7 cm to 4.0 cm in its maximal dimension [2, 3]. All reported sclerosing perineuriomas have had an excellent course without recurrence or metastasis. Malignant transformation has not been reported. Therefore, local excision is considered adequate therapy.

The diagnosis requires light-microscopic, ultrastructural and immunohistochemical examination. Grossly, the tumor is a well-circumscribed and nodular or ovoid firm mass [2, 4, 5]. Microscopically, the tumor is hypocellular with an extensively collagenized stroma and contains small epithelioid and plump spindle cells showing a characteristic corded or whorled growth pattern [2]. Perineurioma cells immunohistochemically express vimentin and EMA and lack immunoreactivity for S-100 protein [2]. Hirose et al. reported that the expression of GLUT1 was specific to perineurial cells and useful to distinguish perineurial cells from other nerve sheath cells [6]. In our two cases GLUT1 showed strongly positive staining, similar to previous results [3].

Since sclerosing perineurioma is not a widely recognized entity, its features on diagnostic imaging, including MRI, have not been previously reported. In the present cases, the tumors showed signal intensity similar to that of muscle on T1-weighted SE MR images and very low signal intensity on T2-weighted FSE MR images. After gadolinium administration, the lesions were partially enhanced in case 1 and diffusely enhanced in case 2. It is known that areas of low signal intensity on T2-weighted MR images can be seen with hemosiderin deposition or with areas of decreased cellularity and dense collagen deposition [7]. The present tumors histologically contained abundant collagen and hyalinized stroma, which were consistent with areas of low signal intensity on T2-weighted MR images. MRI clearly delineated the depth of the tumor and its relationship to the flexor digitorum profundus tendon, aiding in surgical planning. In each of these cases the tumor was exophytically attached to the flexor digitorum profundus tendon and was surrounded by a thin capsule or pseudocapsule, which was confirmed histologically. In our two cases, GLUT1 was strongly positive immunohistochemically.

On MRI, the differential diagnosis of sclerosing perineurioma includes giant cell tumor of tendon sheath, fibroma, neurofibroma, proliferative fasciitis, myxofibrosarcoma, myxoinflammatory fibroblastic sarcoma and clear cell sarcoma, all of which may show low signal intensity on T2-weighted MR images [7–10].

In summary, we have described the MRI features of two cases of sclerosing perineurioma in the left palm and in the left ring finger of young patients.

Awareness of this rare tumor with a short T2 and a predilection for the digits and palms would prompt the interpreter to include sclerosing perineurioma in the differential diagnosis. An excision with tendon-sparing surgery appears to result in cure.

References

1. Lazarus SS, Trombetta LD. Ultrastructural identification of a benign perineurial cell tumor. Cancer 1978;41:1823–9
2. Fetsch JF, Miettinen M. Sclerosing perineurioma: a clinicopathologic study of 19 cases of a distinctive soft tissue lesion with a predilection for the fingers and palms of young adults. Am J Surg Pathol 1997;21:1433–42
3. Yamaguchi U, Hasegawa T, Hirose T, et al. Sclerosing perineurioma: a clinicopathological study of five cases and diagnostic utility of immunohistochemical staining for GLUT1. Virchows Arch 2003;443:159–63
4. Canales-Ibarra C, Magarinos G, Olsoff-Pagovich P, Ortiz-Hidalgo C. Cutaneous sclerosing perineurioma of the digits: an uncommon soft-tissue neoplasm. Report of two cases with immunohistochemical analysis. J Cutan Pathol 2003;30:577–81
5. Huang HY, Sung MT. Sclerosing perineuriomas affecting bilateral hands. Br J Dermatol 2002;146:129–33
6. Hirose T, Tani T, Shimada T, Ishizawa K, Shimada S, Sano T. Immunohistochemical demonstration of EMA/GLUT1-positive perineurial cells and CD34 positive fibroblastic cells in peripheral nerve sheath tumors. Mod Pathol 2003;116:293–8
7. Sundaram M, McGuire MH, Schajowicz F. Soft tissue masses: histologic basis for decreased signal (short T2) on T2-weighted MR images. AJR 1987;148:1247–50
8. Karasick D, Karasick S. Giant cell tumor of tendon sheath: spectrum of radiologic findings. Skelet Radiol 1992;21:219–24
9. Horcajadas AB, Lafuente JL, de la Cruz Burgos R, et al. Ultrasound and MR findings in tumor and tumor-like lesions of the fingers. Eur Radiol 2003;13:672–85
10. Kato K, Ehara S, Nishida J, et al. Rapid involution of proliferative fasciitis. Skelet Radiol 2004;33:300–2

Glut-1 expression and enhanced glucose metabolism are associated with tumour grade in bone and soft tissue sarcomas: a prospective evaluation by [^{18}F]fluorodeoxyglucose positron emission tomography

Ukihide Tateishi[1,6], Umio Yamaguchi[2], Kunihiko Seki[3], Takashi Terauchi[4], Yasuaki Arai[1], Tadashi Hasegawa[5]

[1] Divisions of Diagnostic Radiology, National Cancer Center Hospital, 5-1-1, Tsukiji, Chuo-Ku, 104-0045 Tokyo, Japan
[2] Orthopedic Division, National Cancer Center Hospital, Tokyo, Japan
[3] Division of Clinical Pathology, National Cancer Center Hospital, Tokyo, Japan
[4] Division of Radiology, Research Center for Cancer Prevention and Screening, National Cancer Center, Tokyo, Japan
[5] Department of Clinical Pathology, Sapporo Medical University School of Medicine, Sapporo, Japan
[6] Division of Nuclear Medicine, National Cancer Center Hospital, 5-1-1, Tsukiji, Chuo-Ku, 104-0045 Tokyo, Japan

Received: 21 September 2005 / Accepted: 24 November 2005

Abstract. *Purpose*: This study was conducted to investigate whether ^{18}F-fluorodeoxyglucose (FDG) uptake, quantified by positron emission tomography (PET), correlates with histological variables including tumour grade, cell proliferation, cell cycle control integrity and glucose metabolism in patients with bone and soft tissue sarcomas.
Methods: Eighty-two patients clinically suspected of having a bone or soft tissue sarcoma underwent FDG PET within 1 week prior to operation and 63 patients (mean age 48 years, range 18–74 years) were enrolled in the complete analysis. We excluded 17 patients with pathologically confirmed benign tumours and two patients with uncontrolled diabetes or concomitant malignancy from data analysis. Maximum and average standardised uptake values (SUVs) of the primary lesion were compared with histological variables including tumour differentiation, the presence of necrosis, MIB-1 score, mitotic score, p53 overexpression, MIB-1 grade, mitotic grade and GLUT-1 expression.
Results: Significant correlations were found between maximal and mean SUVs and MIB-1 grade, mitotic grade, MIB-1 score, tumour differentiation and mitotic score. The mean and maximal SUVs were significantly higher in tumours with p53 overexpression than in those without p53 overexpression ($p<0.0001$). GLUT-1-positive tumours had significantly higher mean (6.5±4.2 vs 1.1±0.2, $p=0.006$) and maximal SUVs (8.8±5.4 vs 1.7±0.5, $p=0.005$) than the GLUT-1-negative tumours. GLUT-1 intensity correlated positively with both mean ($r=0.500$, $p<0.0001$) and maximal SUVs ($r=0.509$, $p<0.0001$). Mu ltiple linear regression analysis showed a significant correlation between maximal SUV and MIB-1 grade ($p<0.0001$).
Conclusion: The enhanced glucose metabolism, as determined by SUV, is a strong index of tumour grade in bone and soft tissue sarcomas.

Eur J Nucl Med Mol Imaging
DOI 10.1007/s00259-005-0044-8

Ukihide Tateishi (✉)
Divisions of Diagnostic Radiology,
National Cancer Center Hospital,
5-1-1, Tsukiji, Chuo-Ku,
104-0045 Tokyo, Japan
e-mail: utateish@ncc.go.jp
Tel.: +81-3-35422511, Fax: +81-3-35423815

Introduction

Bone and soft tissue sarcomas are rare malignant tumours which display great variation in histological type. While bone and soft tissue sarcomas are associated with a high mortality, better histological diagnosis and tumour grading are essential for correct treatment decisions and improved patient outcome [1]. Grading is performed according to a scheme based on tumour differentiation, amount of necrosis and number of mitotic figures [1, 2]. A Japanese grading system that uses the MIB-1 score instead of the mitotic score has recently been proposed as the most significant independent predictor of outcome [3, 4].

Optimal management of bone and soft tissue sarcomas depends on their anatomical site, size, growth pattern and tumour stage at the time of initial presentation, and the site, size, growth pattern, and tumour stage are best determined by cross-sectional imaging studies. Accurate imaging studies that provide additional information for tumour grading may be useful in the management of patients with

bone and soft tissue sarcomas [5]. Positron emission tomography with 2-[^{18}F]fluoro-2-deoxy-D-glucose (FDG PET) provides a means of non-invasive quantitative assessment of tumour glucose metabolism in vivo, and enhanced uptake reflects tumour aggressiveness in patients with bone and soft tissue sarcomas and has been used for diagnosis and grading of tumour type [6–10]. This suggests that FDG uptake may be one of the useful biomarkers for identifying aggressive tumours that require intensive treatment protocols and adequate evaluation of therapeutic response. However, there is a need to better understand the underlying mechanism of enhanced FDG uptake and the meaning of high uptake values in clinical settings.

The glucose transfer mediated by glucose transporter protein 1 (GLUT-1) plays a pivotal role in the development and malignant behaviour of cancer cells [11–16]. GLUT-1 belongs to the sugar transporter family and is the dominant protein expressed in cancer cells. It has been found to be overexpressed in cancer cells and to promote glucose metabolism and FDG accumulation [17–20]. However, GLUT-1 overexpression has never been clearly identified in bone and soft tissue sarcomas, and the relationship between GLUT-1 overexpression and FDG uptake or pathological background, including cellular proliferation activity and tumour grade, has never been systematically analysed. The pioneering study by Ito and co-workers [21] was designed to quantify GLUT-1 expression by human rhabdomyosarcoma cells, and the authors demonstrated that GLUT-1 accounted for a major part of the basal and insulin-stimulated glucose transport in vitro. The significance of GLUT-1 overexpression in bone and soft tissue sarcomas in vivo, however, has remained unexplored.

A prospective evaluation of tumour grade based on the FDG PET findings in patients with bone or soft tissue sarcomas has been reported [9, 10], but to the best of our knowledge the factors that influence FDG PET values, including histological variables, are still unknown. The aim of the present study was to identify the histological variables—including tumour grade, cell proliferation as measured by MIB-1 score, cell cycle control integrity as measured by immunohistochemical staining for p53 and overexpression of GLUT-1—that affect FDG PET values in patients with bone and soft tissue sarcomas.

Materials and methods

Patient eligibility

Eligible patients were aged between 18 and 74 years and had a newly diagnosed tumour that was strongly suspected of being a bone or soft tissue sarcoma. Patients were questioned about the presence of three symptoms: induration, tenderness and numbness. The inclusion criteria for the performance status (PS) were PS 0 or PS 1. Exclusion criteria were active concomitant malignancy, clinical evidence of heart disease, uncontrolled diabetes, other severe complications and pregnancy or lactation. The study conformed to the Declaration of Helsinki, and informed written consent was obtained from each subject.

PET scanning was performed with dedicated PET scanners (ECAT ACCEL; Siemens/CTIMI, Knoxville, TN, USA) within 1 week prior to operation. The transverse field of view was 16.2 cm, and 47 image planes were produced. To correct for photon attenuation, a transmission scan was obtained prior to the emission scan with rotating ^{68}Ge rod sources. Prior to PET study, the patients fasted for at least 6 h. All patients were tested for a normal glucose level (range 80–120 mg/dl) before PET scanning. Emission scans from the base of the head to toes were obtained starting 60–80 min after the intravenous administration of 300–370 MBq ^{18}F-FDG. Images were reconstructed with attenuation-weighted ordered subset expectation maximisation with two iterations and eight subsets by using emission scans and reprojected attenuation maps as inputs.

CT scans were acquired using a stacked multislice acquisition protocol on a 16-detector row (Toshiba Medical Systems, Tokyo, Japan) CT scanner. A series of 5-mm-thick images were obtained with the following scan parameters: 120 kVp, 50–100 mA/rotation, 30–40 cm field of view and 512×512 matrix. The subjects were examined in the supine position, and no contrast material was used. All examinations were performed from the head to the toes. Images were reconstructed by using a standard algorithm. PET/CT fused images were made available and reviewed directly on the screen of the workstation (syngo; Siemens, Knoxville, TN, USA).

Images were reviewed in consensus by two board-certified radiologists who were blinded to clinical or radiological information, using hard-copy images in combination with a multimodality computer platform (syngo; Siemens, Knoxville, TN). The two radiologists reviewed all cases in which their interpretations were discrepant and reached a final decision by consensus. The initial

Table 1. Patient characteristics

Age (yrs)	47.5±2.0
Male/female	45 (71)/18 (29)
Mean size (cm)	9.4±5.4
0–5 (cm)	16 (25)
5–10 (cm)	19 (30)
10– (cm)	28 (45)
Type	
Skeletal tumour	17 (27)
Extraskeletal tumour	46 (73)
Distribution	
Extremities	32 (51)
Trunk	31 (49)
Diagnosis	
Pleomorphic MFH/undifferentiated high-grade pleomorphic sarcoma	20 (33)
Ewing's sarcoma/PNET	9 (15)
Synovial sarcoma	8 (13)
Rhabdomyosarcoma	5 (8)
Myxofibrosarcoma	3 (5)
Extraskeletal myxoid chondrosarcoma	3 (5)
Myxoid liposarcoma	3 (5)
Extraskeletal osteosarcoma	2 (3)
Angiosarcoma	2 (3)
Well-differentiated liposarcoma	2 (3)
Fibrosarcoma	2 (3)
Dedifferentiated liposarcoma	1 (2)

Data are presented as mean±standard deviation (SD). The numbers in parentheses are percentages

MFH malignant fibrous histiocytoma, *PNET* primitive neuroectodermal tumour

review of the attenuation-corrected PET images was performed in transaxial, coronal and sagittal planes. Visual analysis was used, and lesions with abnormal FDG uptake were recorded. Abnormal FDG uptake was defined as uptake higher than the background activity in the soft tissue. Lesions with abnormal FDG uptake were confirmed on PET/CT fused images, and their likely anatomical location was recorded. For semiquantitative analysis of the FDG uptake, regions of interest (ROIs) were manually positioned over the tumour in the transmission image. The ROIs placed on the lesions encompassed all pixels that had uptake values greater than 90% of the maximum uptake. When the tumour was extensively heterogeneous, the ROIs were set to cover all the components of the tumour. After correction for radioactive decay, we analysed the ROIs by computing the standardised uptake value (SUV), and both the maximum pixel value within the ROI (maximal SUV) and the mean SUV were recorded. The average values of mean SUV and maximal SUV for each tumour obtained by the IRSAC reconstruction method were calculated along with SD statistics.

Histology

Pathology specimens of all the patients' tumours were obtained by incisional biopsy after the imaging studies, and histological slides were prepared for diagnosis by two expert pathologists. Whenever necessary, immunohistochemical staining was carried out to confirm the diagnosis or tumour type according to the WHO classification system [1]. Mitotic counts in ten high-power fields were determined and classified into three groups. Tumour specimens were immunostained with the antibody Ki-67 (clone MIB-1; DakoCytomation; diluted 1:100 and autoclaved) and the Ki-67 (MIB-1) labelling index (LI) was estimated by calculating the percentage of Ki-67-positive cell nuclei among 1,000 tumour cells in the region of the tumour in which the greatest density of Ki-67 staining was observed under a light microscope. Both the MIB-1 grade (the Japanese grading system) and the mitotic grade (the modified French system) are three-grade systems obtained by summing the scores of tumour differentiation, tumour necrosis and the MIB-1 score or mitotic score, each of which is given a score of 0, 1, 2 or 3 [4, 22]. The tumour differentiation score according to histological type was modified slightly from the French system [22]. The mitotic figures were counted on routine haematoxylin and eosin-stained sections. The areas selected for cell counting were in the most mitotically active parts of the tumours, usually located at the periphery. The mitotic score was obtained by counting the number of mitotic figures in ten consecutive high-power fields. The MIB-1 score was estimated by calculating the percentage of MIB-1-positive cell nuclei among 1,000 tumour cells in the region of the tumour with the greatest density of staining, which in most instances corresponded to the area with the highest mitotic activity. In this study, the histological grade of the tumour was determined by using a three-grade system in which tumour differentiation, tumour necrosis and MIB-1 LI were each given a score of 0, 1, 2, or 3 and the scores were added together [3, 4]. Lesions with MIB-1 LIs of 0–9%, 10–29%, and greater than 30% were assigned MIB-1 scores of 1, 2 and 3, respectively. The three separate scores were added together to produce a combined grade: lesions whose total score was 2 or 3 were classified as grade 1, those whose total score was 4 or 5, as grade 2, and those whose total score

Table 2. Pathological variables and SUVs

	No.	Maximal SUV	*p* Value	Mean SUV	*p* Value
MIB-1 grade*			<0.0001		<0.0001
1	13 (21)	2.6±1.6		1.7±1.1	
2	11 (17)	5.2±3.2		3.6±2.8	
3	39 (62)	11.1±5.0		8.2±3.8	
Mitotic grade*			<0.0001		<0.0001
1	15 (24)	3.3±2.6		2.5±2.6	
2	11 (17)	7.7±5.4		4.8±3.4	
3	37 (59)	10.5±5.2		7.9±4.0	
Differentiation*			<0.0001		<0.0001
1	8 (13)	3.3±2.3		2.2±1.6	
2	13 (21)	4.1±3.3		2.8±2.7	
3	42 (67)	10.5±5.2		7.8±4.0	
Necrosis			0.539		0.366
0	49 (78)	8.1±6.0		5.8±4.5	
1	9 (14)	9.9±4.3		7.6±3.7	
2	5 (8)	7.6±2.6		5.6±3.2	
MIB-1 score*			<0.0001		<0.0001
1	16 (25)	2.8±1.7		1.8±1.1	
2	9 (14)	7.2±4.3		5.0±3.4	
3	38 (60)	10.9±5.1		8.1±3.9	
Mitotic score*			0.006		0.002
0	2 (3)	6.5±7.1		3.1±2.9	
1	25 (40)	5.9±4.9		4.3±4.0	
2	6 (10)	6.8±3.5		4.6±2.2	
3	30 (48)	10.7±3.5		8.0±4.2	

Data are presented as mean±SD. The numbers in parentheses are percentages

*Significant differences ($p<0.05$) were found between groups by the Kruskal-Wallis test. Significant differences were found for MIB-1 grade 1 vs 3, MIB-1 grade 2 vs 3, mitotic grade 1 vs 2, mitotic grade 1 vs 3, mitotic grade 2 vs 3, differentiation 1 vs 3, differentiation 2 vs 3, MIB-1 score 1 vs 3, MIB-1 score 2 vs 3, mitotic score 0 vs 2, mitotic score 0 vs 3, mitotic score 1 vs 2, and mitotic score 1 vs 3

was 6, 7 or 8, as grade 3. Grade 3 tumours were classified as "high grade", and grade 1 and 2 tumours as "low grade". According to this MIB-1 system, tumours were assigned grades 1–3.

A mouse monoclonal antibody (clone DO7; Dako; diluted 1:1,000) was used to immunostain tumour specimens for the p53 epitope located between amino acids 19 and 26 of wild-type and mutant human p53 proteins. p53 overexpression was defined as present when more than 20% of the tumour cells contained nuclei that were immunostained. For GLUT-1, the primary antibody applied was an affinity-purified goat polyclonal antibody (A3536; Dako; diluted 1:500). The intensity of GLUT-1 staining was quantified with regard to the percentage of cells stained. Intensity of GLUT-1 staining was scored as 0 (0%), 1 (1–9%), 2 (10–29%) or 3 (greater than 30%). The p53 overexpression and intensity of GLUT-1 staining were reviewed by two expert pathologists unaware of the clinical information. The final determination of p53 overexpression and intensity of GLUT-1 staining was made by consensus.

Statistical analysis

The demographic variables and imaging characteristics of patients were analysed for statistically significant differences using the χ^2 or Fisher's exact test for categorised variables. A comparison of differences was performed by the two-sample t test. The Kruskal-Wallis test was used to evaluate the differences between the groups defined by each grade. The predictive performance of SUV was evaluated by receiver operating characteristic (ROC) analysis, and areas under the curve were represented by the A_z values. The correlations between pathological parameters and SUV were analysed by Pearson correlation coefficient analysis and multiple linear regression analysis. A p value of <0.05 was considered to indicate a statistically significant difference.

Results

Eighty-two patients clinically suspected of having a bone or soft tissue sarcoma underwent FDG PET, but 19 failed to meet the criteria. One patient had active concomitant malignancy and heart failure. In another patient, the diabetes was uncontrolled before randomisation. Seventeen patients were excluded because they had benign bone or soft tissue lesions: haemangioma (n=4), inflammatory change (n=4), neurinoma (n=3), haematoma (n=2), lipoma (n=1), fibrous dysplasia (n=1), enchondroma (n=1) and giant cell tumour of the tendon sheath (n=1). The remaining 63 patients were the subjects of the complete analysis.

The characteristics of the patients are shown in Table 1. The median age at the time of presentation was 53 years, and seven patients were under 20 years of age. The tumour was located in an extremity in 24 patients and in the trunk in 36 patients. The median tumour size was 9.4 cm, and tumour size ranged from 1.2 to 24.0 cm. Patients in each tumour grade were similar with regard to age, gender, size and tumour location. No significant differences in mean and maximal SUVs were observed between the distribution of the tumour (trunk versus extremities) and tumour size. No significant correlation was observed between tumour size and the mean or maximal SUV. There were 46 extraskeletal tumours and 17 skeletal tumours; there were

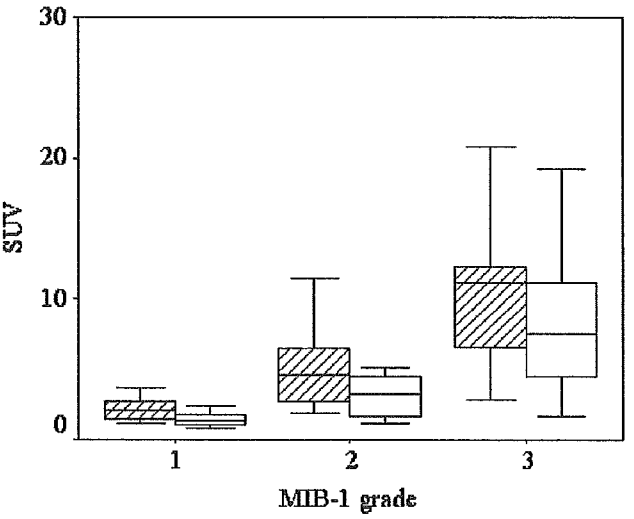

Fig. 1. The relationship between MIB-1 grade and the maximal (*hatched bars*) and mean SUV (*open bars*). Using the Kruskal Wallis test, significant differences were found between MIB-1 grades 1 and 3 and between MIB-1 grades 2 and 3 with respect to both maximal and mean SUV (p<0.05)

no significant differences in mean and maximal SUVs between extraskeletal and skeletal tumours.

Kruskal-Wallis analysis showed significantly different variance in mean and maximal SUV between groups classified by MIB-1 grade (p<0.0001), mitotic grade (p<0.0001), differentiation (p<0.0001) and MIB-1 score (p<0.0001, Table 2). Patients with high-grade tumours had significantly higher mean and maximal SUVs than those with low-grade tumours (p<0.05, Table 2, Figs. 1 and 2). The ROC analyses to predict high-grade tumours revealed A_z values for mean and maximal SUV of 0.926 (95%CI

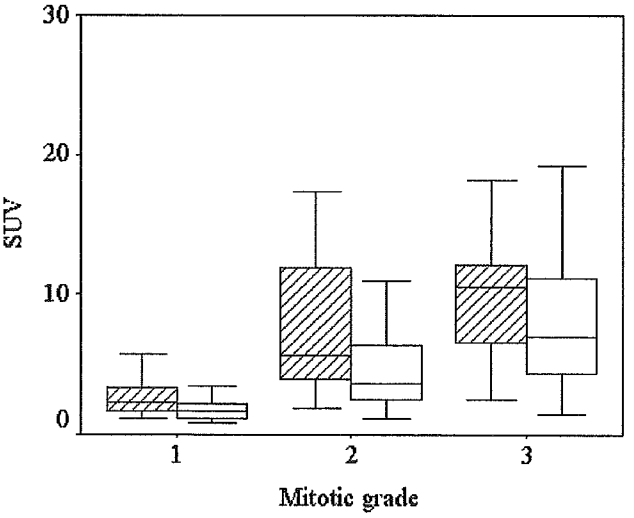

Fig. 2. The relationship between mitotic grade and the maximal (*hatched bars*) and mean SUV (*open bars*). Using the Kruskal Wallis test, significant differences were found between mitotic grades 1 and 3 and between mitotic grades 2 and 3 with respect to both maximal and mean SUV (p<0.05)

0.860–0.992) and 0.919 (0.847–0.991), respectively, by MIB-1 grade, and 0.817 (0.698–0.935) and 0.842 (0.740–0.944), respectively, by mitotic grade.

Visual analysis showed that 59 tumours were positive on FDG PET. All visually negative tumours were MIB-1 grade 1 and mitotic grade 1 (n=4). However, nine tumours with MIB-1 grade 1 and 11 tumours with mitotic grade 1 were visually positive on FDG PET.

It was found that in 49.2% of patients, tumours showed p53 overexpression (Table 3). The mean and maximal SUVs were significantly higher in tumours with p53 overexpression than in those without p53 overexpression (p<0.0001, Table 3, Fig. 3). The ROC analysis to predict tumours with p53 overexpression showed A_z values for mean and maximal SUV of 0.866 (0.776–0.957) and 0.876 (0.787–0.964), respectively.

GLUT-1 was expressed in 92.0% of tumours (Fig. 4). Along with GLUT-1 expression in tumour cells, specific GLUT-1 expression was also found in erythrocytes, perineurium of the peripheral nerves and lymphocytes in the germinal zone. GLUT-1 immunostaining was absent in five tumours: four well-differentiated liposarcomas and one clear cell chondrosarcoma. GLUT-1-positive tumours had significantly higher mean (6.5±4.2 vs 1.1±0.2, p=0.006) and maximal SUVs (8.8±5.4 vs 1.7±0.5, p=0.005) than the GLUT-1-negative tumours (Table 4, Fig. 5). GLUT-1 intensity correlated positively with both mean (r=0.500, p<0.0001) and maximal SUVs (r=0.509, p<0.0001). There were significant associations between GLUT-1 intensity and MIB-1 grade (p<0.0001), mitotic grade (p<0.0001), differentiation (p<0.0001), MIB-1 score (p<0.0001) and mitotic score (p<0.0001, Table 5).

The univariate analysis revealed positive correlations between both mean and maximal SUVs and mitotic grade, MIB-1 grade, mitotic score and tumour differentiation, but the correlation between both mean and maximal SUVs and the degree of necrosis was not significant (Table 6). Multiple linear regression analysis showed a significant correlation between maximal SUV and MIB-1 grade (p<0.0001).

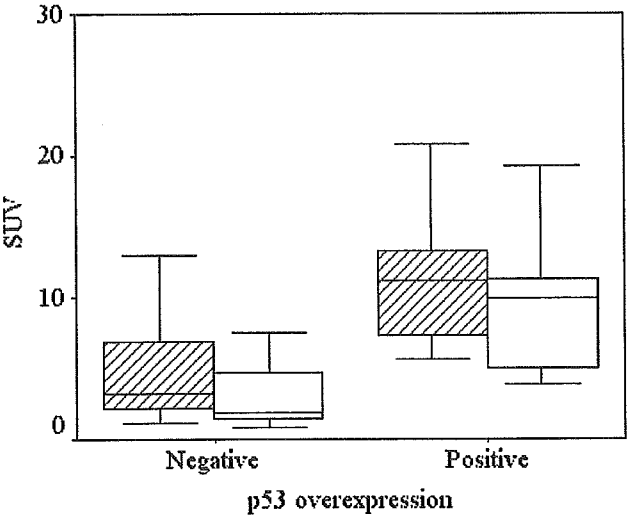

Fig. 3. The relationship between the presence or absence of p53 overexpression and the maximal (*hatched bars*) and mean SUV (*open bars*). A significant difference was found in both groups (p<0.0001)

Table 3. p53 overexpression, SUVs and pathological variables

	Overexpression (+)	Overexpression (−)	p Value
No.	31 (49)	32 (51)	
Maximal SUV*	11.7±5.1	5.0±3.7	<0.0001
Mean SUV*	8.8±3.7	3.5±3.1	<0.0001
MIB-1 grade**			<0.0001
1	0	13 (21)	
2	1 (2)	10 (16)	
3	30 (48)	9 (14)	
Mitotic grade**			<0.0001
1	1 (2)	14 (22)	
2	2 (3)	9 (14)	
3	28 (44)	9 (14)	
Differentiation**			<0.0001
1	1 (2)	7 (11)	
2	1 (2)	12 (19)	
3	29 (46)	13 (21)	
Necrosis**			0.006
0	19 (30)	30 (48)	
1	7 (11)	2 (3)	
2	5 (8)	0	
MIB-1 score**			<0.0001
1	0	16 (25)	
2	2 (3)	7 (11)	
3	29 (46)	9 (14)	
Mitotic score**			<0.0001
0	0	2 (3)	
1	6 (10)	19 (30)	
2	2 (3)	4 (6)	
3	23 (37)	7 (11)	

Data are presented as mean±SD. The numbers in parentheses are percentages

*Significant difference was found between two groups by two-sample t test; **significant difference was found between two groups by Fisher's exact test

Discussion

The results of this study showed that, in patients with bone and soft tissue sarcoma, FDG uptake was significantly correlated with MIB-1 grade, mitotic grade, MIB-1 score, mitotic score and tumour differentiation. The enhanced metabolic response in patients with bone and soft tissue sarcoma is characterised by both increased GLUT-1 staining intensity and p53 overexpression.

Previous studies have shown that increased FDG uptake has a significant correlation with tumour grade in patients with bone and soft tissue sarcomas and that the maximal SUV quantified by FDG uptake is the most reliable predictor of high-grade bone and soft tissue sarcoma [6, 7].

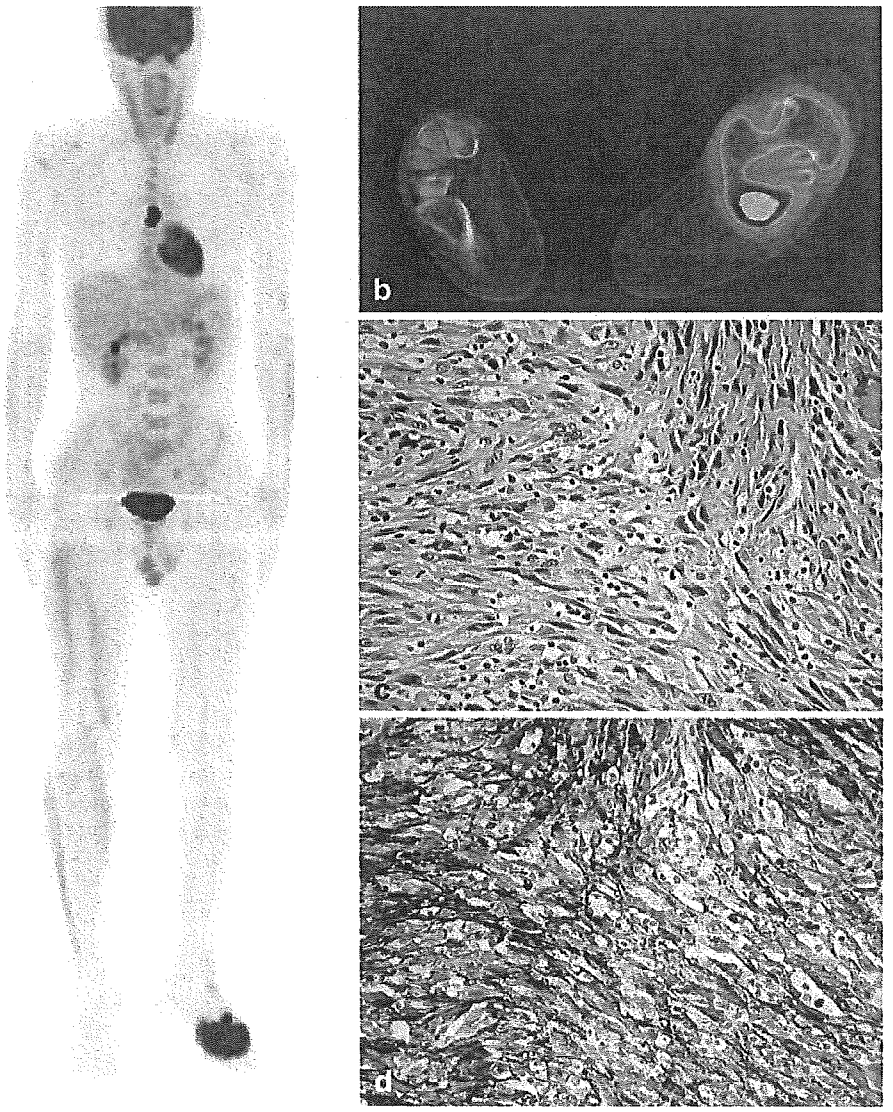

Fig. 4. Pleomorphic malignant fibrous histiocytoma (MFH)/ undifferentiated high-grade pleomorphic sarcoma. **a** PET. Coronal maximum intensity projection image of a 33-year-old man with increased accumulation in the primary tumour of the left foot and sternal metastasis. **b** Co-registered PET and CT images. The tumour shows a maximal SUV of 14.6 and a mean SUV of 11.6. **c, d** Paraffin sections obtained from the tumour demonstrate tumour cells with marked nuclear pleomorphism (**c** haematoxylin-eosin stain) and overexpression of GLUT-1 (**d** GLUT-1 intensity: 3). Tumour shows high-grade features, with MIB-1 grade 3, mitotic grade 3, differentiation 3, necrosis 2, MIB-1 score 3, mitotic score 3 and overexpression of p53

Overexpression of GLUT-1 is the common mediator of glucose uptake in neoplastic cells that supports increased glucose metabolism and promotes neoplastic cells in hypoxic areas. The present study, by demonstrating that there is amplification of GLUT-1 expression when FDG accumulation by tumours increases, builds upon the recent findings of Folpe et al., who suggested a significant correlation between FDG uptake and proliferative activity and cell cycle control integrity in bone and soft tissue sarcomas [8]. The results of the present study may appear to be consistent with the previous studies showing a relationship between glucose metabolism and tumour grade in bone and soft tissue sarcoma [9]. However, most of these studies reviewed cases of bone and soft tissue sarcomas by means of retrospective analyses, and lacked evaluation of GLUT-1 expression [10]. Our study goes beyond earlier observations by showing that FDG uptake is associated with tumour grade as well as with GLUT-1 expression.

Table 4. GLUT-1 intensity and SUV

GLUT-1 intensity	No.	Mean SUV	Maximal SUV
0	5 (8)	1.1±0.2	1.7±0.5
1	4 (6)	2.6±1.3	3.9±1.7
2	16 (25)	4.8±3.5	6.6±4.2
3	38 (60)	7.6±4.2	10.3±5.6

Data are presented as mean±SD. The numbers in parentheses are percentages

Significant differences were found in GLUT-1 intensity 0 vs 1, 0 vs 2, 0 vs 3, 1 vs 3 and 2 vs 3 ($p<0.05$)

Among the factors relevant to tumour grading, MIB-1 grade appeared to contribute most significantly to the enhanced glucose metabolism in patients with bone and soft tissue sarcoma. MIB-1 expression, which is confined

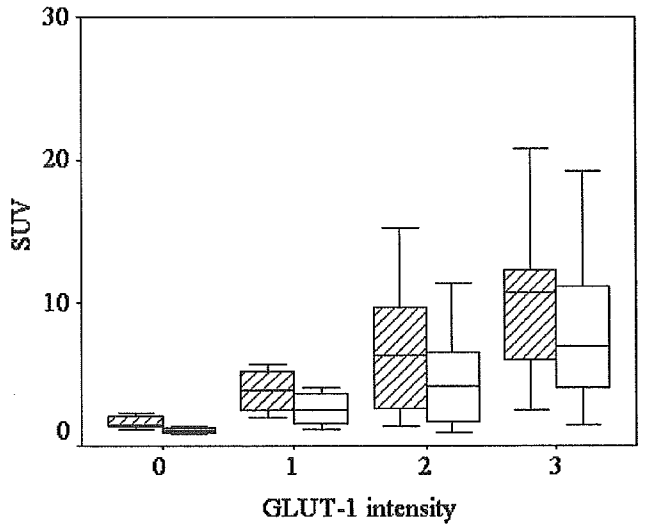

Fig. 5. The relationship between GLUT-1 intensity and the maximal (*hatched bars*) and mean SUV (*open bars*). Using the Kruskal Wallis test, significant differences were found between GLUT-1 intensities 0 and 1, GLUT-1 intensities 0 and 2, GLUT-1 intensities 0 and 3, GLUT-1 intensities 1 and 3, and GLUT-1 intensities 2 and 3 with respect to both maximal and mean SUV ($p<0.05$)

to the late G_1, S, M and G_2 phases of the cell cycle, has traditionally been considered an independent predictor of poor outcome [3]. As pointed out in our previous study, it is conceivable that the MIB-1 grading system has better predictive value than the MIB-1 score and standard grading or staging in the main histological types of soft tissue sarcoma [4]. Therefore, FDG, which reflects proliferative activity, has the potential to stage bone and soft tissue sarcomas. The recent observation of a relationship between enhanced glucose metabolism and the MIB-1 labelling index supports this observation [8]. On the other hand, our results indicate that it is also possible that a more relevant correlation exists between enhanced glucose metabolism and MIB-1 grade.

Our observation of a significant association between enhanced glucose metabolism and p53 overexpression appears to be consistent with the report by Folpe et al., who demonstrated correlations between SUVs and measures of cell cycle control integrity [8]. However, in comparison with previous studies, our study had significant differences that may have influenced our results. The incidence of p53 overexpression in soft tissue sarcoma has been reported to range from 9% to 41% [23–25]. In contrast, we found p53 overexpression in 49% of patients with grade 2 or 3

Table 5. GLUT-1 intensity and pathological variables

	GLUT-1 intensity				*p* Value
	0	1	2	3	
MIB-1 grade*					<0.0001
1	5 (8)	2 (3)	4 (5)	2 (3)	
2	0	2 (3)	4 (5)	5 (8)	
3	0	0	8 (13)	31 (49)	
Mitotic grade*					<0.0001
1	5 (8)	2 (3)	5 (8)	3 (5)	
2	0	2 (3)	4 (5)	5 (8)	
3	0	0	7 (11)	30 (48)	
Differentiation*					<0.0001
1	4 (6)	0	1 (2)	3 (5)	
2	1 (2)	3 (5)	6 (10)	3 (5)	
3	0	1 (2)	9 (14)	32 (51)	
Necrosis					0.719
0	5 (8)	4 (6)	13 (21)	27 (43)	
1	0	0	2 (3)	7 (11)	
2	0	0	1 (2)	4 (6)	
MIB-1 score*					<0.0001
1	5 (8)	2 (3)	7 (11)	2 (3)	
2	0	2 (3)	2 (3)	5 (8)	
3	0	0	7 (11)	31 (49)	
Mitotic score*					0.009
0	1 (2)	0	0	1 (2)	
1	4 (6)	3 (5)	8 (13)	10 (16)	
2	0	1 (2)	3 (5)	2 (3)	
3	0	0	5 (8)	25 (40)	

The numbers in parentheses are percentages
*Significant difference was found between two groups by Fisher's exact test

Table 6. Correlations between SUV and pathological variables

	Maximal SUV	*p* Value	Mean SUV	*p* Value
MIB-1 grade	0.649	<0.0001	0.65	<0.0001
Mitotic grade	0.534	<0.0001	0.547	<0.0001
Differentiation	0.544	<0.0001	0.547	<0.0001
Necrosis	0.035	0.787	0.057	0.657
MIB-1 score	0.626	<0.0001	0.64	<0.0001
Mitotic score	0.402	<0.001	0.428	<0.0001

tumours. This observation is in line with the results of the study by Folpe et al., who demonstrated p53 overexpression in 45% of patients with bone and soft tissue sarcoma, among whom the proportion with grade 2 or 3 tumours was 65% [8]. However, in addition to the higher proportion of patients with p53 overexpression in our study, there were other potentially relevant differences in patient populations.

Like every imaging study, our study had certain limitations. First, the degree of necrosis within the tumour was not paralleled by enhanced glucose metabolism. This suggests that the presence of microscopic necrosis itself may not play a significant role in FDG accumulation. However, when imaging studies of hypoxia, which is strictly linked to tumour necrosis, are considered together, the presence of necrosis is found to be associated with FDG measurements. In addition, there may be inflammatory influences on FDG accumulation, because necrosis within tumour is often associated with macrophage activation. Second, there were five GLUT-1-negative tumours with FDG accumulation. In fact, many glucose transporters exist and are associated with various kinds of malignant tumour [26]. It is possible that GLUT-1-negative tumours would have been positive for other transporters, such as GLUT-3 or GLUT-4. Third, the eight patients with benign tumours were not included in the complete analysis, and this may have influenced the results by exaggerating the high metabolic rates in bone and soft tissue sarcomas. However, enhanced glucose metabolism is also observed in benign bone and soft tissue tumours, including giant cell tumours, because of their proliferative activity and the productive potential of the intercellular matrix [27–29]. Finally, the different uptake time in each patient may have been a source of bias; delayed scan may cause an increase in maximal SUV, such that the actual SUV may have been overestimated in our study.

In conclusion, patients with bone and soft tissue sarcomas have an enhanced glucose metabolism which is correlated with tumour grade. The enhanced glucose metabolism is also associated with increased GLUT-1 staining intensity and with p53 overexpression by the tumour, suggesting a role for this enhanced metabolic response in the evaluation prior to therapy.

Acknowledgements. We thank Hiromitsu Daisaki, Takeshi Murano, and Masashi Suzuki for helping to develop the criteria for the technical quality of the FDG PET/CT imaging; Tetsuo Maeda and Mototaka Miyake for assisting with the literature search; and Yasuo Beppu, Hirokazu Chuman, Akira Kawai and Fumihiko Nakatani for assisting with clinical information. This work was supported in part by grants from Scientific Research Expenses for Health and Welfare Programs, No. 17-12, the promotion and standardization of diagnostic accuracy in PET/CT imaging and BMS Freedom to Discovery Grant. This work was also supported by Travel Grant of the Princess Takamatsu Cancer Research Fund.

References

1. Weiss SW, Goldblum JR Enzinger and Weiss's soft tissue tumors. 4th edn. St. Louis: Mosby, 2001
2. Costa J, Wesley RA, Glastein E, Rosenberg SA The grading of soft tissue sarcomas. Results of a clinicopathologic correlation in a series of 163 cases. Cancer 1984;53:530–541
3. Hasegawa T, Yamamoto S, Yokoyama R, Umeda T, Matsuno Y, Hirohashi S Prognostic significance of grading and staging systems using MIB-1 score in adult patients with soft tissue sarcoma of the extremities and trunk. Cancer 2002;95:843–851
4. Hasegawa T, Yamamoto S, Nojima T, Hirose T, Nikaido T, Yamashiro K, et al. Validity and reproducibility of histologic diagnosis and grading for adult soft-tissue sarcomas. Hum Pathol 2002;33:111–115
5. Bredella MA, Caputo GR, Steinbach LS Value of FDG positron emission tomography in conjunction with MR imaging for evaluating therapy response in patients with musculoskeletal sarcomas. AJR Am J Roentogenol 2002;179:1145–1150
6. Nieweg OE, Pruim J, van Ginkel RJ, Hoekstra HJ, Paans AM, Molenaar WM, et al. Fluorine-18-fluorodeoxyglucose PET imaging of soft-tissue sarcoma. J Nucl Med 1996;37:257–261
7. Eary JF, Conrad EU, Bruckner JD, Folpe A, Hunt KJ, Mankoff DA, et al. Quantitative [F-18]fluorodeoxyglucose positron emission tomography in pretreatment and grading of sarcoma. Clin Cancer Res 1998;4:1215–1220
8. Folpe AL, Lyles RH, Sprouse JT, Conrad EU 3rd, Eary JF (F-18) fluorodeoxyglucose positron emission tomography as a predictor of pathologic grade and other prognostic variables in bone and soft tissue sarcoma. Clin Cancer Res 2000;6:1279–1287
9. Ioannidis JP, Lau J ^{18}F-FDG PET for the diagnosis of soft-tissue sarcoma: a meta-analysis. J Nucl Med 2003;44:717–724
10. Bastiaannet E, Groen H, Jager PL, Cobben DC, van der Graaf WT, Vaalburg W, et al. The value of FDG-PET in the detection, grading and response to therapy of soft tissue and bone sarcomas; a systematic review and meta-analysis. Cancer Treat Rev 2004;30:83–101
11. Chung JK, Lee YJ, Kim SK, Jeong JM, Lee DS, Lee MC Comparison of [^{18}F]fluorodeoxyglucose uptake with glucose transporter-1 expression and proliferation rate in human glioma and non-small-cell lung cancer. Nucl Med Commun 2004;25 (1):11–17
12. Mamede M, Higashi T, Kitaichi M, Ishizu K, Ishimori T, Nakamoto Y, Yanagihara K, Li M, Tanaka F, Wada H, Manabe T, Saga T [^{18}F]FDG uptake and PCNA, Glut-1, and hexokinase-II expressions in cancers and inflammatory lesions of the lung. Neoplasia 2005;7:369–379
13. Brown RS, Leung JY, Fisher SJ, Frey KA, Ethier SP, Wahl RL Intratumoral distribution of tritiated-FDG in breast carcinoma: correlation between Glut-1 expression and FDG uptake. J Nucl Med 1996;37(6):1042–1047

14. Reske SN, Grillenberger KG, Glatting G, Port M, Hildebrandt M, Gansauge F, et al. Overexpression of glucose transporter 1 and increased FDG uptake in pancreatic carcinoma. J Nucl Med 1997;38:1344–1348
15. Higashi T, Tamaki N, Honda T, Torizuka T, Kimura T, Inokuma T, et al. Expression of glucose transporters in human pancreatic tumors compared with increased FDG accumulation in PET study. J Nucl Med 1997;38:1337–1344
16. Higashi T, Saga T, Nakamoto Y, Ishimori T, Mamede MH, Wada M, et al. Relationship between retention index in dual-phase ^{18}F-FDG PET, and hexokinase-II and glucose transporter-1 expression in pancreatic cancer. J Nucl Med 2002;43: 173–180
17. Kunkel M, Reichert TE, Benz P, Lehr HA, Jeong JH, Wieand S, et al. Overexpression of Glut-1 and increased glucose metabolism in tumors are associated with a poor prognosis in patients with oral squamous cell carcinoma. Cancer 2003;97: 1015–1024
18. Kato H, Takita J, Miyazaki T, Nakajima M, Fukai Y, Masuda N, et al. Correlation of 18-F-fluorodeoxyglucose (FDG) accumulation with glucose transporter (Glut-1) expression in esophageal squamous cell carcinoma. Anticancer Res 2003;23: 3263–3272
19. Yen TC, See LC, Lai CH, Yah-Huei CW, Ng KK, Ma SY, et al. ^{18}F-FDG uptake in squamous cell carcinoma of the cervix is correlated with glucose transporter 1 expression. J Nucl Med 2004;45:22–29
20. Kurokawa T, Yoshida Y, Kawahara K, Tsuchida T, Okazawa H, Fujibayashi Y, et al. Expression of GLUT-1 glucose transfer, cellular proliferation activity and grade of tumor correlate with [F-18]-fluorodeoxyglucose uptake by positron emission tomography in epithelial tumors of the ovary. Int J Cancer 2004;109:926–932
21. Ito S, Nemoto T, Satoh S, Sekihara H, Seyama Y, Kubota S Human rhabdomyosarcoma cells retain insulin-regulated glucose transport activity through glucose transporter 1. Arch Biochem Biophys 2000;373:72–82
22. Guillou L, Coindre JM, Bonichon F, Nguyen BB, Terrier P, Collin F, et al. Comparative study of the National Cancer Institute and French Federation of Cancer Centers Sarcoma Group grading systems in a population of 410 adult patients with soft tissue sarcoma. J Clin Oncol 1997;15:350–362
23. Kawai A, Noguchi M, Beppu Y, Yokoyama R, Mukai K, Hirohashi S, et al. Nuclear immunoreaction of p53 protein in soft tissue sarcomas. A possible prognostic factor. Cancer 1994;73:2499–2505
24. Latres E, Drobnjak M, Pollack D, Oliva MR, Ramos M, Karpeh M, et al. Chromosome 17 abnormalities and TP53 mutations in adult soft tissue sarcomas. Am J Pathol 1994;145:345–355
25. Toffoli G, Doglioni C, Cernigoi C, Frustaci S, Perin T, Canal B, Boiocchi M p53 overexpression in human soft tissue sarcomas: relation to biological aggressiveness. Ann Oncol 1994;5: 167–172
26. Medina RA, Owen GI Glucose transporters: expression, regulation and cancer. Biol Res 2002;35:9–26
27. Strauss LG, Dimitrakopoulou-Strauss A, Koczan D, Bernd L, Haberkorn U, Ewerbeck V, et al. ^{18}F-FDG kinetics and gene expression in giant cell tumors. J Nucl Med 2004;45: 1528–1535
28. Borbely K, Fulham MJ, Brooks RA, DiChiro G PET-fluorodeoxyglucose of cranial and spinal neuromas. J Nucl Med 1992;33:1931–1934
29. Beaulieu S, Rubin B, Djang D, Conrad E, Turcotte E, Eary JF Positron emission tomography of schwannomas: emphasizing its potential in preoperative planning. AJR Am J Roentogenol 2004;182:971–974

Disease activity and ^{18}F-FDG uptake in organising pneumonia: semi-quantitative evaluation using computed tomography and positron emission tomography

Ukihide Tateishi[1], Tadashi Hasegawa[2], Kunihiko Seki[3], Takashi Terauchi[4], Noriyuki Moriyama[4], Yasuaki Arai[1]

[1] Division of Diagnostic Radiology, National Cancer Center Hospital, Tsukiji, Chuo-ku, 104-0045 Tokyo, Japan
[2] Department of Clinical Pathology, Sapporo Medical University School of Medicine, Sapporo, Japan
[3] Pathology Division, National Cancer Center Hospital, Tokyo, Japan
[4] Division of Radiology, Research Center for Cancer Prevention and Screening, National Cancer Center, Tokyo, Japan

Received: 29 August 2005 / Accepted: 5 January 2006

Abstract. *Purpose*: The present study was conducted to evaluate whether ^{18}F-fluorodeoxyglucose positron emission tomography (FDG-PET) in combination with computed tomography (CT) reflects disease activity in patients with organising pneumonia.
Methods: Eighty-eight subjects who were normal (n=66) or who had proven organising pneumonia (n=22) underwent FDG-PET and CT imaging. The subjects included 55 men and 33 women, ranging in age from 24 to 63 years (mean 47 years). PET and CT data sets were digitally fused using a conformational PET/CT fusion algorithm. All scans were evaluated independently by two chest radiologists who were unaware of other clinical data. The visual score, maximal and mean standardised uptake value (SUV), and maximal and mean lesion-to-normal tissue ratio (LNR) were calculated. The imaging results were compared with the laboratory and pulmonary function test results. The inflammatory cells in the lesions were quantified immunohistochemically.
Results: The visual score, maximal and mean SUV, and maximal and mean LNR of the patients with organising pneumonia were significantly higher than those of the normal subjects. The patients with air-space consolidation had a significantly higher SUV than those without air-space consolidation (mean±SD 3.08±0.39 vs 2.35±0.56; p<0.05). The number of CD45$^+$ cells was positively correlated with the maximal SUV (r=0.632, p<0.01) and the maximal LNR (r=0.453, p<0.05). The number of CD8$^+$ T lymphocytes also showed positive correlations with the maximal SUV (r=0.540, p<0.01) and the maximal LNR (r=0.547, p<0.01).
Conclusion: Patients with organising pneumonia have an enhanced FDG accumulation which reflects the degree of disease activity.

Keywords: ^{18}F-FDG PET – CT – Chest medicine – Organising pneumonia – Disease activity

Eur J Nucl Med Mol Imaging
DOI 10.1007/s00259-006-0073-y

Ukihide Tateishi (✉)
Division of Diagnostic Radiology,
National Cancer Center Hospital,
Tsukiji, Chuo-ku,
104-0045 Tokyo, Japan
e-mail: utateish@ncc.go.jp
Tel.: +81-3-35422511, Fax: +81-3-35423815

Introduction

Organising pneumonia is characterised by the presence of buds of granulation tissue in the small airways comprising various degrees of interstitial and alveolar infiltration with mononuclear cells and alveolar macrophages [1–3]. Disease activity is correlated with the histological findings of organising pneumonia, which often reflect the incomplete resolution of inflammation leading to the development of fibrosis. Although the clinical course of organising pneumonia varies, the distinctive features of the sporadic onset of a flu-like illness accompanied by respiratory symptoms are often encountered. Organising pneumonia can also be a major histological reaction in various inflammatory processes, including connective tissue disease, drug reactions and infection [4–8].

Computed tomography (CT) findings in patients with organising pneumonia have been thoroughly described [9–15]. The most frequently observed appearance is a patchy area of air-space consolidation that tends to progress and change location over time [9–11]. A better characterisation of CT findings may help to manage patients with organising pneumonia, and the establishment of a reliable indicator will improve the monitoring of disease activity. However, focal lesions often appear as an ovoid mass in contact with the pleura and resembling lung cancer.

^{18}F-fluorodeoxyglucose (FDG) positron emission tomography (PET) can be effectively employed in patients with thoracic malignancies for diagnosis, staging, monitoring after treatment and the detection of recurrence. Nevertheless, multiple inflammatory processes can induce increased ^{18}F-FDG uptake and create false positive results for thoracic malignancies. Various degrees of ^{18}F-FDG uptake have been reported in infiltrative lung diseases, including idiopathic pulmonary fibrosis, collagen vascular disease-associated interstitial pneumonia, drug-induced pneumonia and radiation pneumonia [16–21]. However, organising pneumonia is not a well-known cause of increased ^{18}F-FDG uptake and the relationship of the increased ^{18}F-FDG uptake to clinical parameters and the pathological background has not been clearly identified.

The pioneering study by Majeski and co-workers examined and quantified the activity and progression of organising pneumonia in neonatally thymectomised CBA/J mice infected with reovirus 1/L [22]. The authors demonstrated that activated T lymphocytes provided a measure of disease activity in situ and concluded that the presence of T lymphocytes in the lung tissues of patients with organising pneumonia might indicate an important role in the modulation of disease progression. This previous report focussed on cellular infiltrates early during the inflammatory response in vitro but did not investigate the chronic behaviour of inflammatory cell subtypes, which are often found in pathological specimens obtained from patients with organising pneumonia.

The aim of the present study was to characterise and quantify disease activity in patients with organising pneumonia using co-registered ^{18}F-FDG PET and CT images and comparing these imaging findings with those obtained in normal controls. We also examined the inflammatory cell infiltrates present in pathological specimens, since the histological subtypes of the inflammatory cells could play a role in the progression of the disease and could be correlated with the co-registered PET and CT findings.

Materials and methods

Twenty-two subjects with organising pneumonia were recruited from our institution and were matched for age with a group of 66 normal subjects. ^{18}F-FDG PET and CT were performed in all subjects in a systematic search for cancer, reflecting current practice in our country. A review of the pathological records confirmed that a diagnosis of organising pneumonia had been established in each patient by either a trans-bronchial lung biopsy (n=18) or an open lung biopsy (n=4). Among the subjects with organising pneumonia, ten exhibited cryptogenic organising pneumonia, nine exhibited organising pneumonia associated with collagen-vascular disease and three exhibited drug-induced organising pneumonia. The causative drugs were non-steroidal anti-inflammatory drugs, as determined by history of drug exposure in addition to a lymphocyte stimulation test with the drug in question. Subjects with a history of malignancy, diabetes, respiratory failure, heart failure or liver disease were not eligible for enrolment in this study.

None of the subjects with organising pneumonia had received any therapy prior to the present study. Pulmonary function tests, including measurements of forced vital capacity (FVC), FEV_1, functional residual capacity (FRC), residual volume (RV), total lung capacity (TLC) and carbon monoxide diffusing capacity (D_{LCO}), were performed using a computerised spirometer. The results were expressed in relation to the predicted values for age and height. Venous blood was obtained for routine blood tests, including the determination of C-reactive protein (CRP) levels and white blood cell counts (WBC). The serum concentration of KL-6, a circulating glycoprotein that is a sensitive marker of organising pneumonia (normal value less than 520 U/ml), was also determined. The present study conformed with the Declaration of Helsinki, and informed written consent was obtained from each subject. This study was approved by the local ethics committees after confirming that the subjects had provided their informed consent to a review of their medical records and images.

CT scans were acquired using a stacked multislice acquisition protocol on a 16 detector row CT scanner (Toshiba Medical Systems, Tokyo, Japan). A series of 1.0- and 5-mm-thick images were obtained using the following scan parameters: 120 kVp, 200–250 mA/rotation, 30–40 cm of field of view (FOV) and a 512×512 matrix. The subjects were examined while in a supine position, and none received a contrast material. Thin-section CT images were obtained using 2.0-mm sections reconstructed at 2.0-mm intervals by means of a high spatial frequency algorithm and were retrospectively retargeted to each lung with a 20-cm FOV. All examinations were performed from the apex to the base of the lungs. Images were reconstructed using a standard and a high spatial frequency algorithm at a display window width of 2,000 Hounsfield units (HU) and a window centre of −600 HU. All images were obtained with the subject in deep inspiration.

PET scanning was performed using dedicated PET scanners (ECAT ACCEL; Siemens/CTIMI, Knoxville, TN, USA). The transverse FOV was 16.2 cm, and 47 image planes were produced. To correct for photon attenuation, a transmission scan was obtained prior to the emission scan with 68 rotating germanium rod sources. Prior to the PET study, the patients fasted for at least 6 h. All patients were tested to ensure a normal glucose level (range 4.9–6.7 mmol/l) before PET scanning. Emission scans from the base of the skull to the mid-thigh were obtained starting 60–72 min after the intravenous administration of 300–346 MBq of ^{18}F-FDG. Images were reconstructed with attenuation-weighted ordered-subset expectation maximisation with two iterations and eight subsets using the emission scans and reprojected attenuation maps as inputs.

An initial review of the attenuation-corrected PET images was performed using transaxial, coronal and sagittal planes. PET-CT fused images were available and were reviewed directly on the screen of the workstation. The images were reviewed by two board-certified radiologists who were unaware of clinical or radiological information, using hard-copy images in combination with a multimodality computer platform (syngo; Siemens, Knoxville, TN, USA). The observers assessed the presence of air-space consolidation, ground-glass attenuation, bronchial dilatation, small nodular lesions, band-like opacity and perilobular opacity. Areas of air-space consolidation were considered present when the opacity obscured the underlying vessels. Ground-glass attenuation was defined as an area of hazy increased parenchymal attenuation without obscuration of the underlying vascular markings. Small nodular lesions were defined as well-defined nodules less than approximately 10 mm in diameter. Band-like opacity was defined as smooth or irregular lines longer than 20 mm, sometimes forming arcades [11, 12]. Perilobular opacity was defined as linear opacity bordering the lobule, notably the interlobular septa or pleura [13]. Following an initial independent evaluation, the two observers reviewed all cases in which they had discrepant interpretations and reached a final decision by consensus.

Visual scores ranged from 1 to 5 as follows: 1=no sign of abnormality, 2=probably without abnormality, 3=indecisive concerning abnormality, 4=probable abnormality and 5=definite abnormality. For quantitative interpretation, a region of interest (ROI) analysis was performed. The ROI data were used to calculate standardised uptake values (SUVs) on the PET images. The ROI to measure the SUV was drawn to include the whole lesion in subjects with organising pneumonia. In addition, the ROI was used to evaluate the portion of the corresponding lung segment with 4×4 pixels in the control subjects. SUV was determined, according to the standard formula, as the activity in the ROI given in Bq/ml/injected activity in Bq/weight (kg). Additional SUV data were also obtained for a non-diseased segment of the lung. The maximal and mean pixel value with the ROI and the lesion-to-normal lung ratio (LNR) were recorded.

Tissue blocks obtained at biopsy were fixed in 4% formaldehyde using vacuum inflation, embedded in paraffin and processed into 4-μm-thick serial sections. Histochemical analysis was performed on sections stained with haematoxylin-eosin and elastic van Gieson. The infiltration of total leucocytes ($CD45^+$ cells), macrophages ($CD68^+$ cells), $CD4^+$ T lymphocytes and $CD8^+$ T lymphocytes in the pathological specimens was quantified using immunohistochemical analysis. The sections were dewaxed, rehydrated and moistened with phosphate-buffered saline (pH 7.4). They were then pretreated in an autoclave at 121°C for 10 min in 10 mmol/l citrate buffer (pH 6.0) before incubation. Mouse monoclonal antibodies were used to identify leucocytes (CD45, M0701; Dako), macrophages (CD68, M0814; Dako), $CD4^+$ T lymphocytes (CD4, M0834; Dako) and $CD8^+$ T lymphocytes (CD8, M7103; Dako) using an automated immunostaining system (i6000; BioGenex, San Ramon, CA, USA). Ten representative fields from the immunostained sections were obtained per patient and were examined at a magnification of 400× for the quantitative evaluation. Images of these fields were digitised using a digital camera system (Coolpix Microsystem IV; Nikon, Tokyo, Japan) and analysed by image-processing software (Mac Scope; Mitani, Fukui, Japan). The results were expressed as the number of cells per square millimetre of tissue examined. To improve the validity and reproducibility of the findings, the average number of cells per square millimetre was used to assess the results of the immunohistochemical analysis. Histological diagnosis and quantitative evaluation of the immunostained sections were performed by a histopathologist.

Information regarding symptoms and treatment were retrieved from clinical records and official population registries in all patients. The patients with cryptogenic organising pneumonia and organising pneumonia associated with collagen-vascular disease were treated with doses of prednisone of 1.0 mg/kg daily for 1–2 months. Blood was obtained for routine blood tests, including the determination of CRP levels and WBC counts every week after treatment. Follow-up CT and ^{18}F-FDG PET images were obtained 1 month (n=12) and 2 months (n=10) after withdrawal of the implicated drug or steroid therapy.

Statistical analysis

Correlations between the clinical or pathological values and the SUV were summarised using Pearson correlation coefficients. Clinical variables, pulmonary function test results and PET measurements were compared between groups using two-sample t tests. Variables that were not normally distributed were compared using a Wilcoxon W test. A p value of <0.05 was considered statistically significant.

Results

The clinical characteristics and outcomes of all the patients with organising pneumonia and the normal subjects are summarised in Table 1. There were 55 men (63%) and 33 women (37%). The mean age at the time of diagnosis was 47±7 years, ranging from 24 to 63 years. Sixty-eight subjects (77%) were non-smokers. The proportion of non-smokers was similar among women (78%) and men (76%). The proportion of current smokers was smaller in the control group: only two subjects (3%) were active smokers. The D_{LCO} (% predicted) was lower in the patients with organising pneumonia than in the normal subjects. No differences in VC (% predicted), FEV_1 (% predicted) or FEV_1/FVC (%) were seen between the two groups. The patients with organising pneumonia had significantly higher CRP and WBC values, compared with the control group, but their serum KL-6 level was normal. The two groups were similar with regard to age, gender, height, weight, smoking history and oxygen saturation under room air.

The mean visual score of the patients with organising pneumonia was significantly higher than that of the normal subjects (p<0.01). The 22 patients with organising pneumonia had a visual score of greater than 4, whereas the 56 normal subjects had a visual score of less than 2. The median values of maximal SUV, mean SUV, maximal LNR and mean LNR for the entire study population were 0.53 (range 0.40–3.90), 0.38 (0.22–1.12), 0.77 (0.33–7.64) and 0.53 (0.19–2.11), respectively (Table 2). Significant differences in the mean values for all variables were found between the two groups. Significant correlations between the maximal SUV or the maximal LNR and the CRP level

Table 1. Patient characteristics

	Patients with organising pneumonia	Controls	p Value
No. of subjects examined	22	66	
Age (years)	47.3±2.0	46.3±0.8	NS
No. of females/males	10/12	23/43	NS
Smoking history (pack-years)	5.5±1.8	3.5±0.9	NS
VC (% predicted)	90.8±5.9	88.7±1.6	NS
FEV_1 (% predicted)	81.1±5.5	78.4±2.3	NS
FEV_1/FVC (%)	81.5±1.2	83.6±0.7	NS
D_{LCO} (% predicted)	87.9±1.7	92.8±1.1	<0.05
Saturation (%)	99.8±0.1	99.7±0.1	NS
KL-6 (U/ml)	298.6±17.6	268.0±15.0	NS
CRP (mg/dl)	2.4±0.2	0.0±0.0	<0.0001
WBC (/mm^3)	7,271.3±220.5	4,733.2±41.9	<0.0001

Values are expressed as mean ± standard deviation unless otherwise indicated

VC vital capacity, *FEV_1* forced expiratory volume per 1 s, *FVC* forced vital capacity, *D_{LCO}* carbon monoxide diffusing capacity, *CRP* C-reactive protein, *WBC* white blood cell count, *NS* not significant

were seen only in the patients with organising pneumonia. No significant relationships were seen between the PET measurements and the pulmonary function test results, oxygen saturation under room air, serum KL-6 level or WBC.

A good inter-observer agreement was obtained for the analysis of the CT findings (weighted kappa 0.63–0.78). Among the patients with organising pneumonia, common CT findings included air-space consolidation, ground-glass attenuation and bronchial dilatation (Table 3). Air-space consolidation was predominantly peripheral and was often associated with areas of ground-glass attenuation and bronchial dilatation (Fig. 1). Less common CT findings included band-like opacity, small nodular lesions and perilobular opacity. Band-like opacity was predominantly peripheral and located in the lower zone. The patients with air-space consolidation had a significantly higher maximal SUV than those without consolidation (mean±SD 3.08±0.39 vs 2.35±0.56; $p<0.05$). However, no other significant correlations were seen between the maximal SUV and CT findings.

Tissue specimens were characterised according to the presence of granulation comprising variable infiltrates of lymphocytes, macrophages and neutrophils (Fig. 1). The lesions were admixed with fibrin exudates and collagen-containing fibroblasts, embedded in a tissue matrix. Minor infiltration of the lesion by plasma cells and eosinophils was also found. The results of the cell counts in the lesions are shown in Table 4. Increased numbers of leucocytes ($CD45^+$ cells), macrophages ($CD68^+$ cells), CD4 T lymphocytes and CD8 T lymphocytes were observed (Fig. 1). The number of $CD45^+$ cells infiltrating the lesion was positively correlated with the maximal SUV ($r=0.632$, $p<0.01$) and the maximal LNR ($r=0.453$, $p<0.05$, Fig. 2). The number of $CD8^+$ T lymphocytes infiltrating the lesion was positively correlated with the maximal SUV ($r=0.540$, $p<0.01$) and the maximal LNR ($r=0.547$, $p<0.01$, Fig. 3). No significant correlations were found between the numbers of $CD68^+$ cells and $CD4^+$ T lymphocytes infiltrating the lesion and the ^{18}F-FDG PET measurements.

All patients with cryptogenic organising pneumonia or organising pneumonia associated with collagen-vascular disease showed clinical improvement which was defined as an improvement in both CT findings and laboratory examinations. The three patients with drug-induced organising pneumonia responded to withdrawal of the implicated drug. In all patients with organising pneumonia, the median values of maximal SUV (0.65±0.18), mean SUV (0.38±0.16), maximal LNR (0.74±0.26) and mean LNR (0.61±0.21) were decreased with response to withdrawal of the implicated drug or corticosteroid therapy.

Table 2. ^{18} F-FDG PET measurements

	Patients with organising pneumonia	Controls	*p* Value
Visual score	4.70±0.10	1.60±0.10	<0.0001
Mean SUV	1.00±0.02	0.31±0.01	<0.0001
Mean LNR	1.49±0.06	0.48±0.02	<0.0001
Maximal SUV	2.95±0.13	0.49±0.01	<0.0001
Maximal LNR	4.44±0.30	0.75±0.03	<0.0001

Values are expressed as mean ± standard deviation
SUV standardised uptake value, *LNR* lesion-to-normal lung tissue ratio

Discussion

This study shows that a significant increase in ^{18}F-FDG uptake occurs in the parenchymal lesions of patients with organising pneumonia. The enhanced ^{18}F-FDG accumulation in patients with organising pneumonia is characterised by increased numbers of $CD45^+$ cells and $CD8^+$ T lymphocytes in the parenchymal lesion and is associated with the presence of air-space consolidation on PET/CT fused images. The significant correlations between the maximal SUV and various cellularities suggest that ^{18}F-FDG accumulation in the lungs of these patients reflects the degree of disease activity.

Previous studies have shown the predictive value of the glucose metabolic rate in patients with pulmonary inflammation [16–19]. Inflammatory cells produce ATP at a level that is several times higher during activation, compared with at baseline. Inflammatory cells, like neutrophils and activated macrophages, at the site of inflammation also show increased ^{18}F-FDG uptake. Using microautoradiography, Kubota et al. showed that newly formed granulation tissues around tumours and macrophages, which are concentrated in the outer zones surrounding the necrotic areas of tumours, significantly accumulated ^{18}F-FDG in vitro [23]. The results of the present study appear to agree with these previous findings for pulmonary inflammation. However, no significant correlations were found between the numbers of $CD68^+$ cells and $CD4^+$ T lymphocytes infiltrating the lesion and the ^{18}F-FDG PET measurements. This may be due to a different inflammatory response from that of outer zones surrounding the necrotic areas of tumours.

The mechanism of abnormal ^{18}F-FDG uptake in patients with organising pneumonia is not clear. Histopathological examinations revealed that the numbers of $CD45^+$ cells and $CD8^+$ T lymphocytes in the parenchymal lesions were positively correlated with the maximal SUV, whereas the numbers of $CD68^+$ cells and $CD4^+$ T lymphocytes infiltrating the lesion were not significantly correlated with the maximal SUV. Pulmonary inflammation can be either acute or chronic, the former showing predominantly neutrophil infiltrates and a few eosinophils and monocytes, whereas $CD68^+$ cells are predominant in the latter [24]. $CD4^+$ and $CD8^+$ T lymphocytes, but not neutrophils, are also the dominant inflammatory cells in chronic inflammatory lesions, whereas neutrophils are attracted to acute phases. In our patients with organising pneumonia, the most active lesions are thought to be in the process of transition from acute to chronic pulmonary

Table 3. CT findings of organising pneumonia

CT finding	No. (%)
Air-space consolidation	18 (82)
Ground-glass attenuation	17 (77)
Bronchial dilatation	16 (73)
Band-like opacity	11 (50)
Small nodular lesion	10 (45)
Perilobular opacity	6 (27)

inflammation. These findings are in agreement with the concept that ^{18}F-FDG uptake in inflammatory lesions is dependent on the presence of leucocytic or lymphocytic masses capable of binding the radioisotope.

The maximal SUV was associated with increased cellularity in the pathological specimens, the latter being characteristic of the active inflammatory process in organising pneumonia. In cases with organising pneumonia, the generalised signs of inflammation are frequently masked; however, our patients with organising pneumonia had higher CRP levels and WBCs than the control group. These findings support the use of the maximal SUV for staging active inflammation in organising pneumonia. A possible way to evaluate the contribution of the maximal SUV to staging of the disease would be to investigate the correlation between maximal SUV and clinical parameters, such as pulmonary function tests and CT findings. The increase in the number of inflammatory cells was not always paralleled by the CT patterns of organising pneumonia, as shown by the lack of any association between the maximal SUV and the five CT findings other

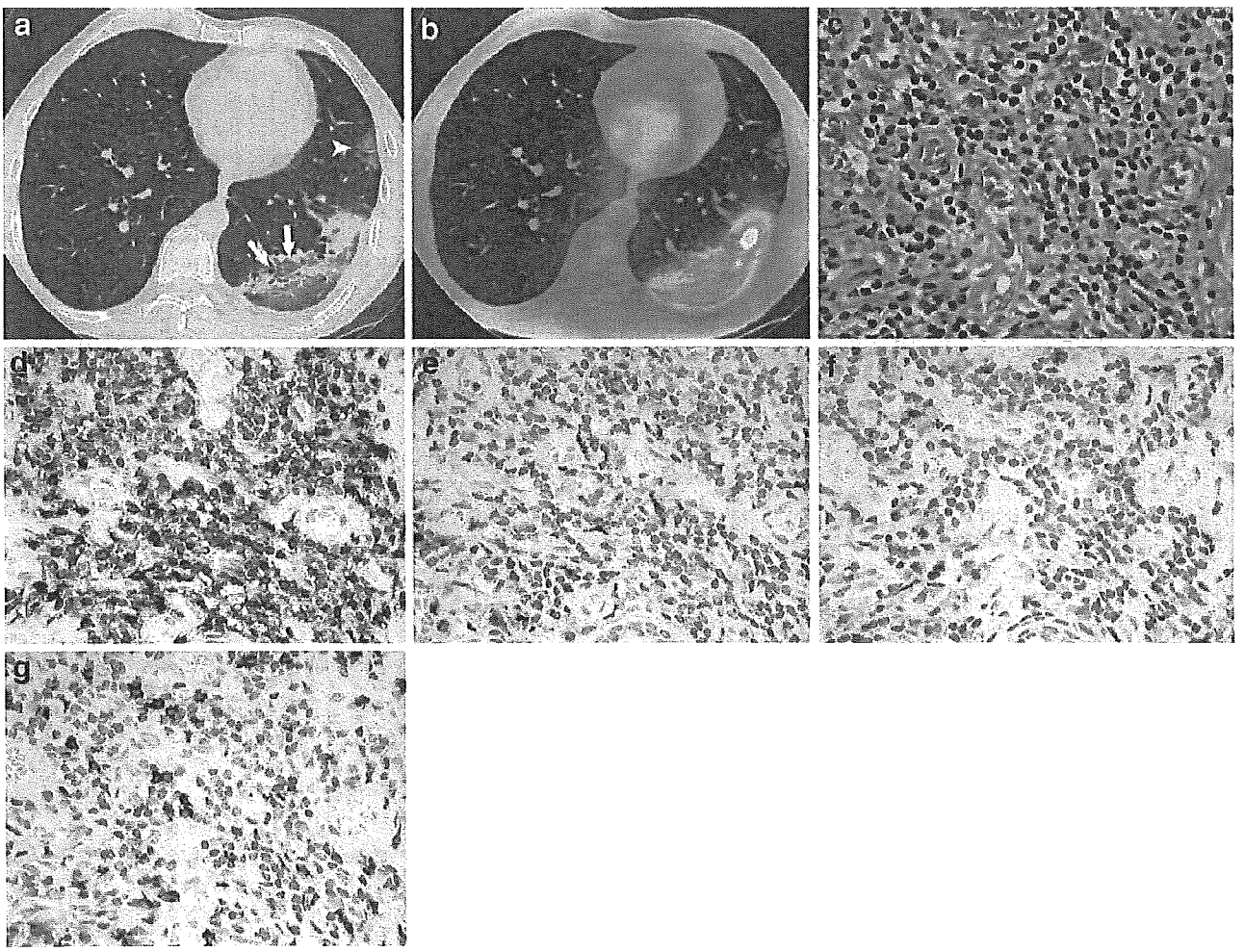

Fig. 1. a. Transverse CT scan through the lower lung lobes in a 54-year-old man with cryptogenic organising pneumonia. Air-space consolidation is visible in the periphery with areas of ground-glass attenuation and bronchial dilatation (*arrows*). A discrete patchy area of ground-glass attenuation is also visible (*arrowhead*). **b** Co-registered PET and CT image shows abnormal ^{18}F-FDG uptake within the lesion. **c** Photomicrograph of the pathological specimen shows inflammatory cells in an excessive proliferation of granulation tissue (haematoxylin-eosin stain, original magnification ×200). **d–g** Immunostainings with monoclonal antibodies anti-CD45 (**d**), anti-CD68 (**e**), anti-CD4 (**f**) and anti-CD8 (**g**) show numerous positive cells within the lesion. Increased numbers of leucocytes ($CD45^+$ cells), macrophages ($CD68^+$ cells), CD4 T lymphocytes and CD8 T lymphocytes were seen (original magnification ×200)